Single Molecule Spectroscopy Studies of Acid-Base Chemical Gradients using Nile Red as a Probe of Local Surface Acidity

Abdulhafiz Usman^a, Shelby L. Weatherbee^b, Maryanne M. Collinson^b, Keith L. Hohn^{a,c,*}, Daniel
A. Higgins^{d,*}

^aDepartment of Chemical Engineering, Kansas State University, Manhattan, KS 66506 ^bDepartment of Chemistry, Virginia Commonwealth University, Richmond, VA 23284 ^cDepartment of Chemical, Paper, and Biomedical Engineering, Miami University, Oxford, OH 45056

^dDepartment of Chemistry, Kansas State University, Manhattan, KS 66506

Abstract

Single molecule spectroscopy studies of local acidity along bifunctional acid-base gradients are reported. Gradients are prepared by directional vapor phase diffusion and subsequent reaction of 3-aminopropyl-trimethoxysilane with a uniform silica film. Gradient formation is confirmed by spectroscopic ellipsometry and by static water contact angle measurements. X-ray photoelectron spectroscopy is used to characterize the nitrogen content and degree of nitrogen protonation along the gradient. Nile Red is employed as the probe dye in single molecule spectroscopy studies of these gradients. While Nile Red is well-known for its solvent sensitivity, it is used here, for the first time, to sense the acid/base properties of the film in two-color widefield fluorescence imaging experiments. The data reveal broad bimodal distributions of Nile Red emission spectra that vary along the gradient direction. The single-molecule results are consistent with solution-phase ensemble acid/base studies of the dye. The former reveal a gradual transition from a surface dominated by basic aminosilane sites at the high-amine end of the gradient to one dominated by acidic silanol sites at the low-amine end. The sub-diffractionlimited spatial resolution afforded by superlocalization of the single molecules reveals spatial correlations in the acid/base properties of the gradient over ~ 200 nm distances. These studies provide data relevant to the use of aminosilane-modified silica in bifunctional, cooperative chemical catalysis.

^{*}Corresponding author emails: higgins@ksu.edu and hohnkl@miamioh.edu

INTRODUCTION

Bifunctional catalysts are frequently found to be superior to their monofunctional analogues, with enhanced catalytic activities and selectivities attributable to cooperativity between the chemically distinct sites on their surfaces. Silica materials incorporating both inorganic and organic functional groups comprise one class of bifunctional materials now being widely explored.1 Oftentimes, the bifunctionality of these materials derives from the presence of both acidic and basic surface sites. The acidic sites may comprise weakly acidic silanol groups inherent to the silica surface, or more acidic carboxylic, sulfonic, or phosphoric acids may be attached during materials synthesis.² Similarly, basic sites may be incorporated through covalent attachment of aminosilanes to the silica matrix. Bifunctional acid/base materials are now being investigated for use in the heterogeneous catalysis of aldol,³ nitroaldol,³ Knoevenagel,⁴ and Michael reactions.⁴ While these materials show tremendous promise, a full understanding of their cooperativity has not yet emerged. Further studies of how the acidic and basic sites on the catalyst surface interact with each other and with chemical reagents are needed to better optimize catalyst performance. Of course, the interactions that occur between catalyst sites are determined by their spacing and organization, and the development of new means to control and measure these parameters is also warranted.

One method for controlling the spacing between active sites on the surface of a heterogeneous catalyst for use in fundamental investigations is via the preparation of gradient materials.^{5,6} The surface of a bifunctional acid/base gradient incorporates high concentrations of acid at one end of the gradient and high concentrations of base at the other. A gradual variation in acid and base site concentrations, and hence their proximity to each other, occurs between the two extremes. Silica thin film gradients are now being explored in the literature and are easily

fabricated by a variety of methods.⁷ Physical vapor diffusion is perhaps the simplest to implement, relying on the directional diffusion of precursor vapors over a substrate, and their subsequent reaction with its surface.^{8,9} By controlling the concentration of precursor present in the solvent-filled deposition reservoir, the distance between the reservoir and the substrate, and the time over which deposition occurs, gradients of controlled surface functionality, incorporating gradual variations in catalyst site spacing and interactions can readily be achieved.

Once gradient materials have been obtained, the density and organization of catalytic sites must be characterized. Classical solution-phase acid/base titrations could be used to determine the density of acidic or basic sites, although the implementation of spatially resolved titrations on gradient surfaces would be challenging. Likewise, zeta potential measurements can be used to obtain related information, with similar challenges in making spatially resolved measurements. One spectroscopic method that provides elemental sensitivity and the ability to spatially resolve variations in the surface chemistry is XPS mapping. While XPS has provided valuable information on the interactions between surface sites in recent studies of acidic/basic silica gradients, the spatial resolution achieved is usually on the order of tens of micrometers. Atomic force microscopy, and chemical force microscopy in particular, are also well suited to detecting interactions between acidic and basic surface sites, in this case, with nanometer-scale spatial resolution.

As effective alternatives, fluorescence-based single-molecule detection and spectroscopy experiments hold significant promise for probing the properties of bifunctional catalyst surfaces. Fluorescent probe molecules can serve as proxies for the reagents used in catalytic reactions, revealing the relevant molecular level interactions that occur at active sites with nanometer scale spatial resolution, when detected at the single molecule level. Related methods are now being

widely employed to achieve a better understanding of catalysis. For example, single molecule methods have been implemented in studies of the connection between the static and dynamic properties of catalysts and their reactivity¹² and to characterize reaction kinetics.¹³ They have also been used to study shape-selective catalysis on solid catalysts,¹⁴ the accessibility of Brønsted acid sites on zeolites¹⁵ and agarose gels,¹⁶ transesterification reactions on layered doubled hydroxides,¹⁴ and to explore the thermodynamics of the reversible redox reaction of resorufin on SiO₂ nanospheres.¹⁷ In related work, spectroscopic single molecule detection has been employed to probe the acid/base properties of microporous¹⁸ and mesoporous silica,¹⁹ and aluminosilicate films.²⁰ The latter studies have employed the very few well-known, pH-sensitive indicator dyes available that are also sufficiently fluorescent to detect at the single molecule level.

Nile Red is a highly solvatochromic dye that is commonly used to characterize the polarity of bulk organic solvents. It exhibits a profound bathochromic shift in both its absorption and emission spectra as solvent polarity increases. These spectral shifts are readily quantified and correlated with solvent dielectric properties via Mataga-Lippert theory. Nile Red is also sufficiently fluorescent to allow its detection at the single molecule level, facilitating a variety of studies of materials polarity in local, nanoscale environments within polymer films, and along silica gradients, in the surfactant-filled pores of mesoporous silica films, and within organic nanotubes. While alternative forms of Nile Red have been synthesized and employed to probe the acid/base properties of small organic molecules and nanomaterials, it it attention has been paid to the intrinsic acid/base response of commercial Nile Red itself. To our knowledge, only a single publication has reported its absorption and emission characteristics in the presence of an acid. This previous study

reported a shift in its absorption maximum from ~ 550 nm in pure ethanol to ~ 640 nm upon addition of H_2SO_4 . An isosbestic point was observed at ~ 580 nm. In the same study, the fluorescence quantum yield of the dye was determined to decrease from 0.68 in its unprotonated form to 0.04 when protonated. Modeling studies suggested this response results from protonation of the molecule at the nitrogen atom of its oxazine ring.³²

In this work, bifunctional acid/base chemical gradients were prepared by vapor phase diffusion of 3-aminopropyl-trimethoxysilane (APTMOS) over uniform silica films supported on Reaction of APTMOS with the silica film created a stable aminosilane glass coverslips. gradient. Gradient formation was verified by spectroscopic ellipsometry measurements of film thickness and sessile drop water contact angle measurements of film wettability. The gradients were subsequently characterized by X-ray photoelectron spectroscopy (XPS). XPS mapping provided a measure of film nitrogen content along the gradient direction. A two-component Gaussian function was used to fit the N(1s) XPS spectra, which incorporate peaks centered at 398.9 eV and 400.5 eV. These were attributed to the unprotonated and protonated forms of the aminosilane nitrogen, respectively. The area under the 400.5 eV peak, relative to total peak area was used to probe spatial variations in the fraction of protonated amine along the gradient on sub-millimeter distance scales. Two-color spectroscopic single molecule detection experiments were used to probe gradient acid/base and polarity properties with sub-diffraction-limited spatial resolution.³³ Bimodal distributions of Nile Red emission characteristics were observed. These results are consistent with monotonic spatial variations in the interactions between the basic dye and acidic silanol sites along the gradient. An in-depth analysis of the spatially resolved single molecule emission data was used to explore the length scale over which spatial correlations in gradient acidity and basicity occur. The results obtained and their interpretations are certain to

be of great value to those working to better understand the unique attributes of bifunctional acidbase catalysts

EXPERIMENTAL SECTION

Sample preparation.

Gradient and non-gradient silica films were prepared on glass coverslips (FisherFinest Premium) and on silicon wafers when required (see below). In preparation for gradient deposition, all substrates were first cleaned by rinsing with deionized water and acetone. They were then dried with nitrogen and plasma-cleaned in air for 6 min. A uniform silica base layer was subsequently created by spin-casting a silica sol on the substrate surface. These sols were prepared by mixing tetraethyl orthosilicate (TEOS), spectroscopic grade ethanol, HCl (as a 0.1 M aqueous solution), and deionized water (17.9 M Ω cm), in that order, in mole ratios of 1:90:0.02:6, respectively. The mixture was then stirred for 1 h and aged in a desiccator for 24 h prior to use. Base layer films were obtained by dropping 150 μ L of the sol onto the substrate, which was then spun at 2500 RPM for 30 s. As a final step, the coated substrates were stored in a desiccator for at least 24 h.

Aminosilane gradient films were prepared by vapor phase deposition of 3-aminopropyl-trimethoxysilane (APTMOS) on the silica base layer. Deposition of APTMOS was carried out at ambient laboratory temperature (~ 25° C) in a humidity-controlled Plexiglas chamber. Immediately prior to gradient deposition, each silica base layer was cleaned in an air plasma for 3 min. This process also served to activate the base layer by exposing reactive silanol groups. The activated, base-layer-coated substrate was next placed on an elevated platform in the deposition chamber. For vapor deposition purposes, APTMOS was diluted to a 1:10 ratio (by volume) in toluene. Approximately 200 µL of APTMOS:toluene solution was then transferred

to an open reservoir that was positioned within the chamber at a horizontal distance of 4 mm from the base-layer-coated substrate. The substrate-reservoir distance was optimized to obtain aminosilane films of the desired thickness at the high-amine end of the gradient.³⁴ Each substrate was exposed to APTMOS vapor for a period of 6 min during gradient deposition. The films were then transferred to a vacuum desiccator and maintained under dynamic vacuum overnight to remove any loosely bound silanes.

For single-molecule experiments, the gradient films were doped by spin-casting (2500 rpm, 30s) a dilute (0.1 nM) ethanolic solution of Nile Red on their coated surfaces. Dye-doped films were subsequently stored in a desiccator for at least 24 h prior to use. Aminosilane functionalized gradient films were used as-prepared for ellipsometry, water contact angle (WCA), and X-ray photoelectron spectroscopy (XPS) measurements, without loading the dye.

Instrumentation and methods.

Film thickness. TEOS base layer and aminosilane gradient film thicknesses were measured using a spectroscopic ellipsometer (α -SE, J. A. Woollam). Films employed in thickness measurements were prepared on silicon wafers. All ellipsometry data were fit using the transparent film on silicon model. No allowance was made for film roughness. Measurements were made at 2 mm intervals along each gradient, starting from the high-amine end. Film thickness was measured both prior to and after gradient deposition at approximately the same positions. The former measurement gave the base layer thickness, while the latter yielded the gradient film thickness, after subtraction of the value for the base layer. Replicate measurements were made at \sim 1 mm intervals at the high-amine end and at 2 mm intervals at the low-amine end along the direction perpendicular to the gradient at each point.

Static water contact angle. The water wettability of each gradient film was determined by sessile drop WCA measurements. These experiments were carried out on a home-built contact angle goniometer. Measurements were taken at 3 mm intervals along the gradients by depositing $1~\mu L$ droplets of 17.9 M Ω cm water at each point and photographing the droplets through a zoom lens. Replicate measurements were made at \sim 9 mm spacings along the direction perpendicular to the gradient at each point. Photographs of the droplets were analyzed using a Plugin for the freely-available ImageJ software. ³⁵

Elemental composition. The chemical composition of the gradient films was verified by XPS mapping. These measurements were performed on a PHI VersaProbe III Scanning XPS Microprobe with an Al Kα source (1486.6 eV). XPS data were acquired at 1.5 mm intervals starting from the high amine end (closest to the reservoir). A 200 μm diameter spot size was employed, along with a 55 eV pass energy, and a 0.1 eV step size. All N(1s) peaks were measured relative to the C(1s) peak at 284.6 eV.

Single molecule spectroscopic imaging. Dye-doped aminosilane gradient films were imaged on a wide-field epi-fluorescence microscope that has been described previously.³⁶ Briefly, this microscope is built upon a Nikon TiE inverted light microscope that employs the Nikon Perfect Focus stabilization system. Nile Red fluorescence was excited by 0.5 mW (measured prior to entry into the microscope) of 532 nm laser light derived from a solid-state laser (Coherent Sapphire, 50 mW). The laser light was focused into a spinning optical diffuser prior to entry into the epi-illumination port of the microscope. It was subsequently collected and reflected from an appropriate dichroic beam splitter (Chroma) and focused into the back aperture of a 100X, 1.49 oil immersion objective (Nikon Apo-TIRF), providing an ~ 15 μm diameter illuminated area in the sample under conventional wide-field illumination. Fluorescence from

the dye molecules excited in the sample was collected by the same objective and then separated from the excitation light by passage back through the dichroic beam splitter and a 570 nm longpass filter. The dye emission was next directed into an image splitter (Cairn Research Optosplit II) that divided the signal into separate spectral bands spanning 580 ± 20 nm and 640 ± 20 nm. The image splitter employed a second dichroic beam splitter (Chroma T610lpxr) and 580/40 and 640/40 bandpass filters (Chroma). Fluorescence images in these two spectral bands were simultaneously recorded using an electron-multiplying CCD camera (Andor iXon DU-897). Fluorescence videos were acquired at 2X2 binning using conventional gain only. The videos were 80-100 frames in length. Individual video frames were acquired with a 0.5 s exposure every 0.65 s.

Fluorescence videos were analyzed using spot location/identification software developed in-house in the National Instruments LabView environment. This software has been described previously in more detail. The program was used to separate the two spectral channels in each video, to correct for minor image distortion and offset imparted by the image splitter, and to identify, locate, and link fluorescence spots observed in the individual video frames into trajectories showing any motions and intensity or spectral fluctuations exhibited by each molecule. In locating each molecule, the individual fluorescence spots were fit to 2D Gaussian functions, allowing for the location of each molecule to be determined to a sub-diffraction-limited precision of 50 nm.

Ensemble fluorescence spectroscopy. Fluorescence spectra were acquired from dilute solutions of Nile Red using a conventional fluorimeter (Jobin Yvon-SPEX Fluoromax-2). All spectra were acquired from solutions in 1 cm x 1 cm fused silica cuvettes. Ensemble fluorescence data were also acquired on the same microscope used in single molecule studies. In

this case, a polydimethylsiloxane (PDMS) cell was attached to a plasma-cleaned coverslip and the coverslip placed on top of the microscope (see above) operating in total internal reflection mode. The sample cell was filled with 150 µL of each of a series of solvent mixtures containing Nile Red at 10 nM concentration. The dye was excited by 532 nm laser light (0.5 mW). Fluorescence videos 20-30 frames in length were acquired with a 0.5 s exposure time every 0.65 s. A new coverslip and PDMS cell were used for each solvent mixture to prevent cross contamination of the solutions. The videos were analyzed using the ImageJ software package. The background-subtracted emission intensities for identical rectangular areas in the two spectral channels were used to calculate the emission ratios (E).

RESULTS AND DISCUSSION

Gradient characterization.

Verification that aminosilane gradients were obtained on the silica-baselayer-coated substrates was accomplished by spectroscopic ellipsometry, static WCA measurements, and by XPS mapping. Figure 1a shows ellipsometry data acquired from a representative aminosilane gradient. The data are plotted as a function of position relative to the original location of the deposition reservoir during gradient fabrication. The gradient was measured to be a few molecular layers in thickness (~ 0.5 nm/monolayer)³⁸ at the high-amine end (7 mm). It rapidly thinned to just less than one monolayer at the low-amine end (19 mm).

Figure 1b plots representative WCA data along a similar gradient. The WCA was largest ($\sim 60^{\circ}$) at the high-amine end, due to the greater hydrophobicity associated with its organic functionality, and smallest ($\sim 15^{\circ}$) at the low-amine end. These data are consistent with previously reported WCA results for self-assembled monolayers.³⁹ Together, the ellipsometry

and WCA data provide conclusive evidence that the surface has been modified by the aminosilane and that a chemical gradient has been obtained.

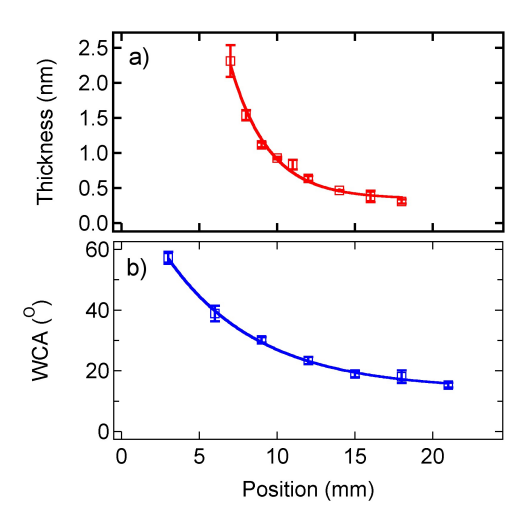


Figure 1. a) Thickness of aminosilane gradient as measured by spectroscopic ellipsometry. b) WCA data acquired by static water contact angle methods. Both measurements are plotted as a function of distance along each gradient, relative to the original position of the reservoir used to prepare the gradients. The error bars represent the experimental standard deviation obtained for three replicate measurements in each case.

More chemically specific information on aminosilane gradient composition was provided by XPS mapping. Figure 2 depicts the results of these studies along a representative gradient, with the raw XPS data shown in Figure 2a. The total nitrogen content of the gradient film was quantified by determining the area under the full N(1s) peak at ~ 400 eV. Importantly, the N(1s) spectra are also sensitive to the protonation state of the nitrogen atom, with unprotonated nitrogen yielding a peak near 398.9 eV and its protonated form found at a higher energy of 400.5 eV. To characterize the protonation state of the amine group, the raw XPS spectra were fit to two-component Gaussian functions (blue lines in Figure 2a) and the area under each of these components separately integrated. While the fitting of XPS data usually requires use of a more physically correct Voigt profile, Gaussian functions serve as a suitable approximation in the present studies, given the signal-to-noise level that could be achieved for the thin film gradients.

Total film nitrogen is plotted in Figure 2b as the full area under each spectrum (i.e., summing both components). These data reveal an approximately ten-fold decrease in film nitrogen content running between the high-amine and low-amine ends. The XPS results are consistent with the film thickness data (Figure 1a) although the latter measurements were initiated further down the gradient. XPS data obtained from uniformly coated aminosilane films and uncoated silica base layers are provided in Supporting Information. These show the lack of a gradient in the former and the absence of detectable nitrogen in the later, as expected.

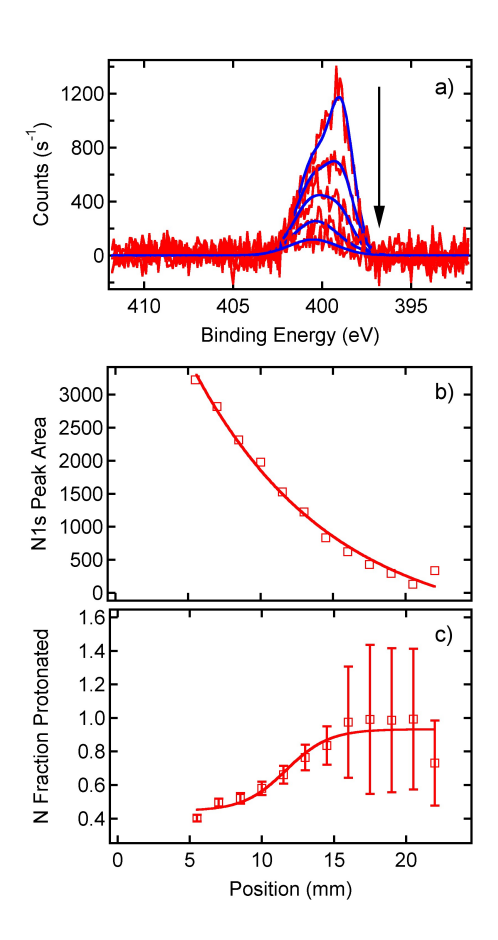


Figure 2. a) N1s XPS spectra (red lines) recorded along an aminosilane gradient at 3 mm spacings (see arrow) starting at the high-amine end of the gradient. Each spectrum was fit to a pair of Gaussian functions (blue lines) centered at 398.9 eV and 400.5 eV, which are assigned to the unprotonated and protonated forms of the aminosilane nitrogen, respectively. b) N1s peak area as a function of position along the same gradient. c) Protonated fraction of aminosilane nitrogen as a function of gradient position. The error bars represent estimates of the standard deviation of each value. The error bar at 19 mm is the average of the error bars at 17.5 and 20.5

mm due to weak signal at this point. All data are plotted as a function of distance relative to the approximate original position of the reservoir used to prepare the gradients.

Figure 2c plots the degree of amine protonation as a function of position along the gradient, as determined from the XPS data. These results show that nitrogen protonation increases with distance from the high-amine end. This reflects a transition along the gradient from regions having a high density of basic amine sites and a low density of acidic silanols (high-amine end) to those incorporating a low density of amine groups and a high density of silanol sites (low-amine end). Unfortunately, the error bars become large at the low-amine end, due to the low density of basic sites in that region. While these data reveal the presence of a gradient in film acidity/basicity, the spatial resolution achieved was on the order of a millimeter.

Nile Red solution-phase ensemble spectroscopy.

As noted above, Nile Red is well known for its strong solvatochromism.²¹ As a result of this sensitivity to the dielectric properties of its surrounding environment, it has been widely employed to characterize the polarity of solvent systems,^{21,42} ionic liquids,⁴³ micelles,^{42,44} proteins,⁴⁵ and DNA,⁴⁶ and has also been used to probe organically-modified silica sols.²² However, its absorption and emission characteristics are also expected to be sensitive to solution/environment acidity. Previous work in this area has, to our knowledge, been restricted primarily to studies of its spectral shift in ethanol upon addition of a strong acid.³²

In the present work, the *acid sensitivity* of Nile Red was further explored by monitoring its emission in a series of mixtures of ethyl acetate and acetic acid. The results are shown in Figure 3a. Ethyl acetate and acetic acid were chosen for these studies because they have similar dielectric constants, ε , of 6.08 and 6.20, respectively.⁴⁷ Little or no polarity-dependent shift in the Nile Red emission spectrum is expected between these two solvents (see below). Instead,

any spectral shift that occurs upon addition of acetic acid to an ethyl acetate solution should be due to acid-base interactions between the acetic acid and the basic dye. Indeed, the data in Figure 3a show a rather significant bathochromic shift in the Nile Red emission spectrum as acetic acid is added to the ethyl acetate solution. Its spectrum is peaked at ~ 585 nm in pure ethyl acetate and at ~ 640 nm in pure acetic acid. No isoemissive point was observed along the series of mixtures. The latter observation is expected, as the spectra obtained in these solvents are relatively broad compared to their separation.

In order to better understand how the acid-dependent spectral shifts of Nile Red might be manifested in single molecule studies (see below), solution-phase ensemble fluorescence data were also acquired on the same microscope used in those studies. The results are shown in Figure 3b. In this case, the fluorescence in each of two spectral bands (580 ± 20 nm and 640 ± 20 nm) was recorded and used in the calculation of an emission ratio, E, as defined in Eqn. 1.²⁸

$$E = \frac{I_{640} - I_{580}}{I_{640} + I_{580}} \tag{1}$$

Here, I_{580} and I_{640} represent the fluorescence signal detected in each of the two spectral bands. A large E is indicative of relatively red emission and a small E value reflects relatively blue emission. The results shown in Figure 3b demonstrate that an abrupt bathochromic shift in the Nile Red emission occurs when relatively small amounts of acetic acid (5%) are added to the ethyl acetate. The fluorescence emission also becomes weaker with increasing acid concentration, as reported previously.³²

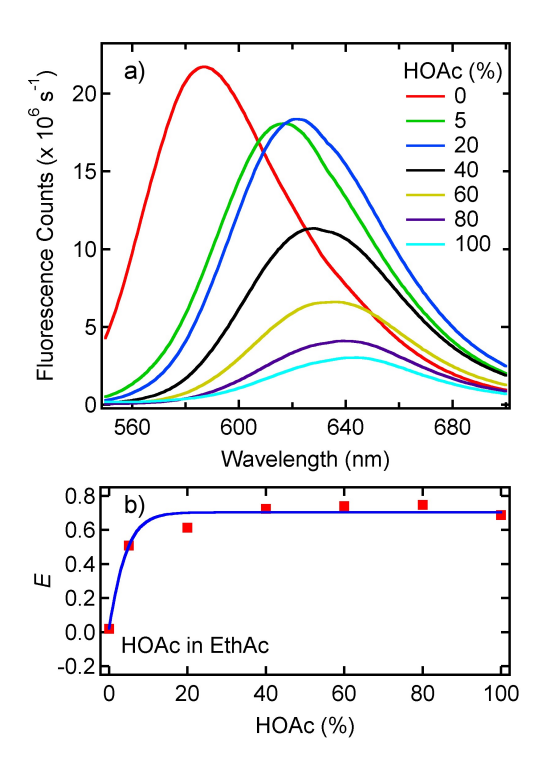


Figure 3. Solution phase ensemble fluorescence from Nile Red in mixtures of ethyl acetate (EthAc) and acetic acid (HOAc). a) Fluorescence spectra obtained as a function of HOAc in EthAc using a conventional fluorimeter. b) Ensemble, solution phase *E* values obtained from Nile Red (10 nM) in a series of HOAc/EthAc mixtures, showing an abrupt change in its emission spectrum with increasing acid concentration. The data in b) were recorded on the same microscope used for single molecule experiments.

The difference in E values expected for Nile Red in ethyl acetate and acetic acid, based on solvent polarity alone, may be estimated using previously reported methods, data, and mathematical relations. This calculation is provided in Supporting Information. Using the solvent dielectric constants given above, a change in E of < 0.01 units is predicted for Nile Red between pure ethyl acetate and pure acetic acid. Importantly, the shift in E for Nile Red shown in Figure 3b is \sim 0.7 units, approximately seventy-fold larger, indicating it reflects primarily a change in protonation state, not a change in solvent polarity.

Nile Red fluorescence is certain to exhibit some dependence on gradient polarity along with the protonation effects described above. Unfortunately, it was not possible to identify a

suitable solution-phase model upon which to predict the exact contributions of polarity variations along the gradient. Rather, the results of our previous work^{28,37} reveal that a change in E of ~ 0.8 units across the full length of the gradient could be expected due to polarity effects alone. While the contributions of variable polarity and dye protonation to the measured E values along the gradient may be difficult to distinguish, it is expected that the effects of molecular-level acid-base interactions will dominate over the polarity effects of the thin aminosilane films in these studies. Since polarity-dependent spectral shifts are based upon the average dielectric properties of the environment surrounding each molecule,^{23,24} they are not expected to be so different in the presence and absence of thin, near-monolayer films.

The response of Nile Red to the presence of acid has been attributed previously to protonation of the dye at the nitrogen heteroatom on its oxazine ring.³² However, in both the non-aqueous environments described above and along the aminosilane gradients, the local dielectric constant is likely too small to support full transfer of a proton to the dye. Rather, it is expected that Nile Red will interact with acids under these conditions by forming a hydrogen bond,⁴⁸ as has been described in previous studies of Nile Red interactions with fluorophenol in nonaqueous media.⁴⁹ Therefore, it is expected that interactions between acidic sites (i.e. silanol groups) along the gradient and the dye will involve the sharing of a proton through a hydrogen bond. Figure 4 shows a schematic depiction of this interaction. Although complete transfer of a proton is not expected, the process will be characterized as protonation or deprotonation of the dye for simplicity in this work.

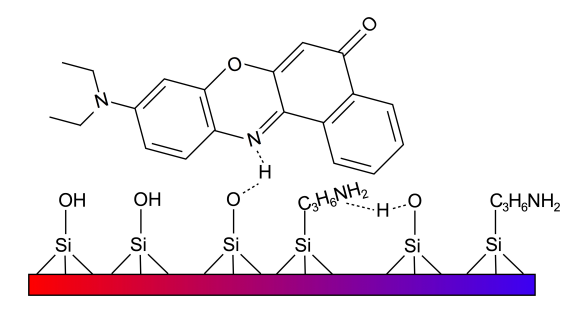


Figure 4. Possible hydrogen bonding interactions (dashed lines between atoms) along the aminosilane gradient. These interactions occur between acidic silanol sites and the basic Nile Red dye and also between acidic silanols and basic amine groups on the gradient surface.

Single molecule spectroscopic imaging.

Single molecule detection and spectroscopic imaging using the Nile Red dye provides a valuable means to further characterize the acid/base properties of the aminosilane gradients at much higher spatial resolution than was achieved by XPS. These experiments were performed by recording wide-field fluorescence videos along the length of Nile-Red-doped aminosilane gradients. Videos were acquired simultaneously in two separate spectral bands, spanning 580 ± 20 nm and 640 ± 20 nm, as was done in earlier single molecule studies of silica film polarity. Figure 5 shows representative fluorescence images obtained at the top (high-amine end) and bottom (low-amine end) of the gradients. These depict the first frame in 50 frame long videos analyzed at each position. The original videos are provided in Supporting Information. Each image incorporates several isolated fluorescent spots attributable to detection of fluorescence from single Nile Red molecules. Assignment of the spots to emission from individual molecules is supported by the extensive "blinking" (i.e., fluorescence intermittency) observed in the original videos (see Supporting Information).

The fluorescence detected from individual molecules in the 580 nm and 640 nm bands varied significantly between individual spots in the data obtained. While many molecules appeared in both images (i.e., 580 nm and 640 nm), others were observed in only one image,

emitting too weakly to be visible in the other. These characteristics were also found to vary with distance along each gradient. As shown in Figure 5, the molecules were generally brighter in 580 nm images acquired at the high-amine end (10 mm position). At the low-amine end (24 mm), they were frequently brighter in the 640 nm channel. In contrast to the solution-phase studies, no clear evidence of a decrease in quantum yield of emission from the dye was found towards the more-acidic, low-amine end of the gradient. The reason for this difference is unknown at present but may derive from a reduction in the rate of nonradiative decay in the more static environment of the gradient surface, compared to the solution phase. These initial observations provide strong evidence of variations in the local film environment probed by each molecule, whether due to acidity or polarity effects.

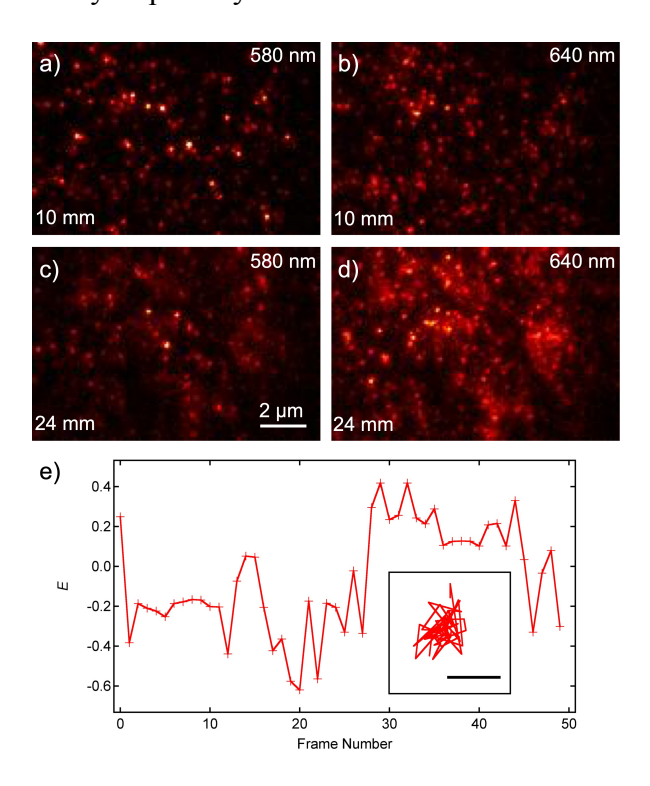


Figure 5. a)-d) Representative images of Nile Red on an aminosilane gradient. The color scale in each image depicts fluorescence counts ranging from 0 - 800 counts per pixel above background. e) Example time transient showing uncommon changes in E attributed to abrupt changes in protonation state of the molecule. This molecule was found in a video acquired at the

14 mm position along the gradient (see Figure 6). The inset shows the X,Y position of the spot across a 50 frame long video segment. The scale bar is 125 nm in length.

The video data also revealed characteristics of the molecules that help in understanding the spectroscopic results. As noted above, the molecules exhibited extensive fluorescence intermittency. However, the videos revealed little if any variation in the spectral characteristics of the fluorescence as the molecules blinked on and off. The video data also demonstrate that the molecules were largely associated with fixed sites along the gradient, moving little if at all, over the ~ 30 s length of each video. These observations are generally expected as the films were imaged under a dry nitrogen atmosphere. They suggest that the local environment probed by each molecule changed little over the course of each video.

To better understand the properties of the local environment surrounding each molecule, a more quantitative analysis of the single molecule data was also performed. This involved precisely locating the individual spots in each of the 580 nm or 640 nm video frames, and linking the detected spots into time trajectories. For this purpose, the intensity profile of each spot was fit to a 2D Gaussian function, providing not only the spot location in X and Y, but also the spot amplitude, giving a direct measure of its intensity. The spot intensities were subsequently used to calculate the emission ratio, E, (see Eqn. 1) for each molecule along its time trajectory. Most such time trajectories revealed few clear variations in E, outside the measurement noise. Trajectory data from one rare counter example are shown in Figure 5 (bottom). In this figure, E is plotted for one molecule across the full length of the video segment in which it was found. These data show three apparent jumps in E between values of \sim -0.3 and \sim 0.2 occurring after frames 1, 27, and 44. The inset shows its spatial trajectory, which reveals that the molecule likely remains fixed on the gradient surface. The apparent variations in its location are

attributable to the limited precision at which the molecule can be located (σ_{xy} = 51 nm). These results indicate the local environment experienced by the molecule was either changing in time or the molecule was hopping on the gradient surface over distances much smaller than the localization precision.

The quantitative assessment of single molecule environments involved acquiring video data at 2 mm spacings along each gradient, beginning at the point from which data collection commenced, 10 mm from the original position of the deposition reservoir during gradient fabrication. This distance corresponds to 6 mm from the edge of the glass substrate. These data were acquired out to a distance of 24 mm from the reservoir in each case. A total of five videos were collected from each location along the gradient at intervals spanning a 7.5 mm range across the gradient. Each experiment was performed on a total of four different gradients. The emission characteristics of thousands of individual Nile Red molecules were obtained and analyzed in these experiments. As noted above, the E values varied little outside measurement noise, so the mean E for each molecule along its trajectory was determined in each case and these mean values were then compiled into histograms depicting variations in the local environment. Histograms of the mean E values from the single molecules were first prepared for each position along and across each gradient. The histograms obtained from each of the five positions across each gradient were next summed together. Finally, those obtained at the same position along each of the four replicate gradients were subsequently summed. The compiled results are shown in Figure 6 and are displayed as a function of position along the gradients.

The distributions shown in Figure 6 reveal a general shift in the single molecule emission characteristics from negative E values at the high-amine end of the gradients (10 mm) to positive E values at the low-amine end (24 mm). As noted above, these results may reflect i) an increase

in the polarity of the local environments, or ii) increased protonation of the Nile Red molecules, both occurring as a function of distance along the gradient. While the participation of both effects is likely, it is noteworthy that the distributions shown in Figure 6 are very broad compared to those obtained previously in similar studies of silica film polarity.^{28,37} Moreover, the distributions shown in Figure 6 appear to be bimodal, while monomodal distributions were observed in previous polarity studies,²⁸ except when Nile Red was concluded to strongly interact with silanol sites on the silica surface.³⁷ The observation of broad, bimodal distributions in the present studies of acid/base gradients is therefore taken as good evidence of the response of Nile Red to variations in the acidity properties of the film. While some contributions from variations in gradient polarity are certainly still present, acid/base effects are believed to dominate.

A simpler view of spatial variations in the properties of the local environments probed along the gradients was obtained by fitting the histogram data shown in Figure 6a-h to two component Gaussian distributions. A global fitting of these data was performed, with the data fit to distributions peaked at $E = -0.35 \pm 0.15$ (deprotonated Nile Red) and $E = 0.67 \pm 0.22$ (protonated Nile Red), with the error bars representing 95% confidence intervals. Limitations in the apparent quality of the individual fits may arise from the presence of more than two components in the distributions, because the distributions do not follow simple Gaussian statistics, or simply because of the limited number of measurements made. Nevertheless, an initial assessment of the gradient properties was obtained by using the amplitudes of the two components (A⁻ and A⁺) to determine the fractional contributions of the protonated dye at E = 0.67 to the overall distribution. This analysis is similar to that performed for the XPS data Figure 2c, which plots the fraction of amine groups protonated at each position along the gradient. The results obtained from the single molecule data, calculated as $A^+/(A^+ + A^-)$, are

plotted in Figure 6i. The plot obtained is remarkably similar to that shown in Figure 2c for the XPS experiments. Both show a dominant transition in gradient properties occurring between 10 and 15 mm along the gradient. It is concluded that the single molecule results depict predominantly the effects of a transition from unprotonated Nile Red dispersed on the gradient surface at the basic, high-amine end of the gradient (10 mm) to protonated Nile Red hydrogen bonded to silanol sites on the gradient surface at the acidic, low-amine end (24 mm).

The single molecule results were subsequently used to obtain high-resolution information on any spatial correlations in film properties. This analysis was performed to obtain a better understanding of the spatial scale over which the acid or base characteristics of the gradient vary. In this analysis, the mean E value obtained from each single molecule was compared pairwise to the E values obtained from every other single molecule detected in the same video. Simultaneously, the distance between the pairs of molecules being compared was also determined. The latter was determined by taking the difference between the average molecular positions, as determined from their trajectories. Scatter plots depicting the differences in E (ΔE) versus the distances between the molecules (Δd) at each position along the gradient were then prepared by compiling all data obtained from each of the five videos acquired across each of the four replicate gradients. These results are shown in Figure 7a,b for the 12 mm and 22 mm positions.

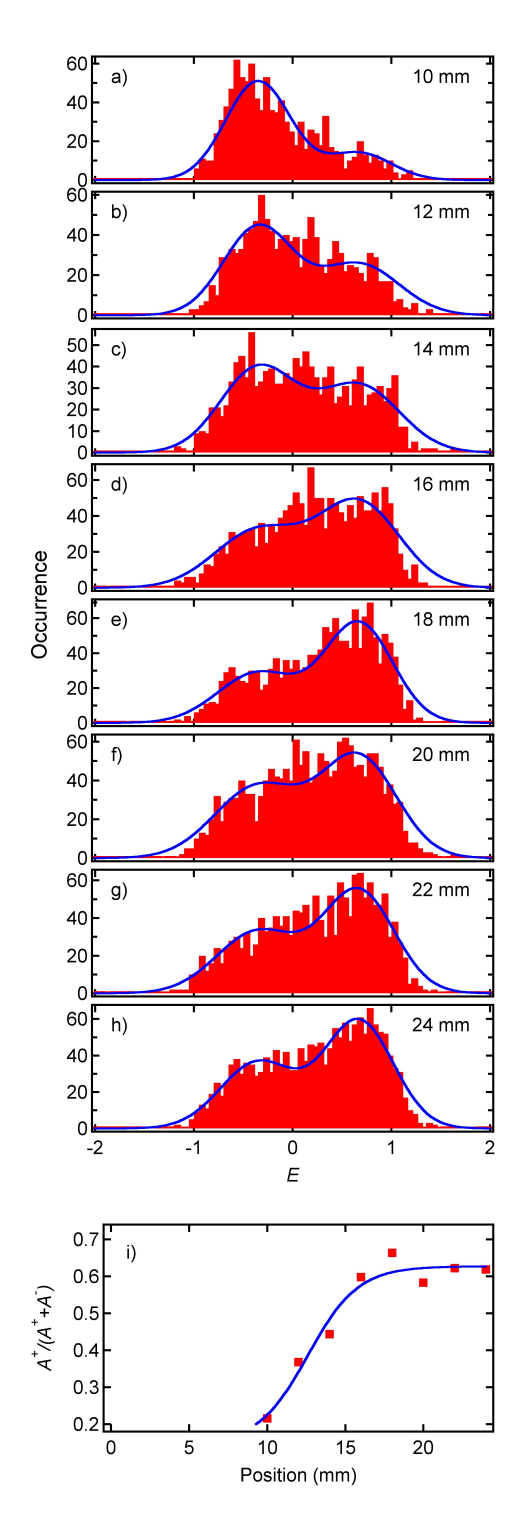


Figure 6. a)-h) Histograms depicting the single molecule emission ratio (red bars) as a function of position along the aminosilane gradient films and the fits of these distributions to two component Gaussian distributions (blue lines). i) Fraction emitting at high E, attributed to the protonated form of Nile Red (red squares) and a fit to the data (blue line) appended to better show the trend with position along the gradient.

The data shown in Figure 7a,b reveal that at large single molecule distances (i.e., $\Delta d > \sim 1$ µm), the E values obtained are completely uncorrelated with each other. However, at small distances (i.e., $\Delta d < \sim 1$ µm), they clearly become correlated, with the range of ΔE values obtained depending on the distance between molecules. To better depict these correlations, the ΔE values were boxcar averaged in 0.025 µm (Δd) wide bins. Figures 7c,d plot these results for the 12 mm and 22 mm positions. These results show that the average ΔE is very close to zero for closely spaced single molecules. Its value then increases gradually to a constant value of ~ 0.6 at distances $> \sim 0.5$ µm.

The observation of an average ΔE near zero for closely spaced molecules is clearly biased by the blinking of the molecules. Molecules that blink are interpreted as different molecules in the present analysis. Rather than attempting to deduce which data represent the same molecule counted multiple times and which are produced by different molecules appearing at approximately the same location at different times, the extent to which blinking molecules contribute to the observed correlation in E values was instead assessed by counting the number of molecules observed in each of the 0.025 μ m wide bins. These data are plotted in Figure 7e,f. The plots show a peak in the number of molecules at $\Delta d = 0$, followed by a drop and then a subsequent rise in their numbers as Δd increases. The peak at $\Delta d = 0$ shows the expected artifact caused by blinking molecules being counted multiple times. Absent this artifact, very few if any molecules would be found at $\Delta d = 0$, assuming random positioning of the molecules. The number of molecules is expected to increase approximately linearly as Δd increases because the probability of finding two molecules at a distance Δd on a two-dimensional surface increases linearly with distance. Note that the apparent scarcity of molecules around $\Delta d = 0.5$ μ m derives

from a combination of the artificially large number of molecules at $\Delta d = 0$ and the expected increase in number of molecules with increasing Δd .

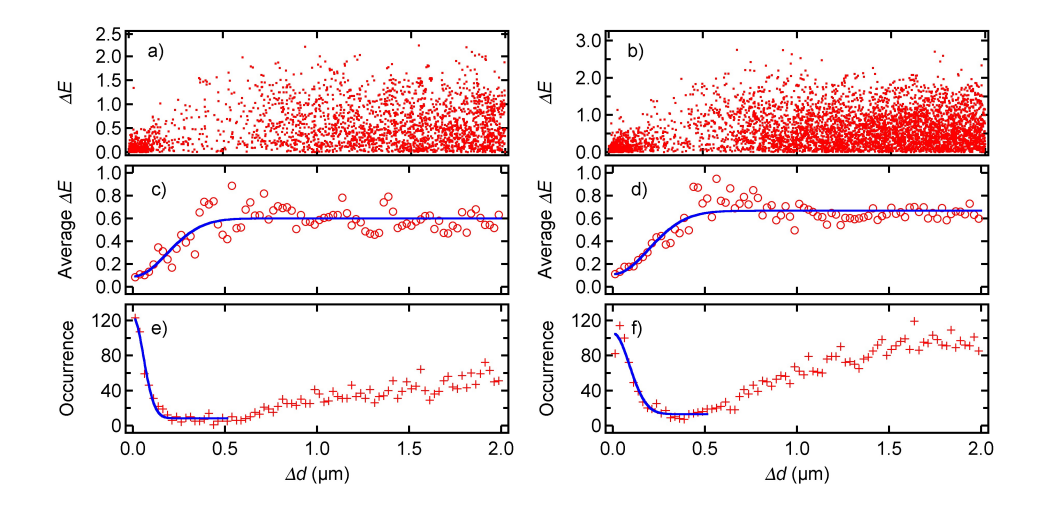


Figure 7. Difference in $E(\Delta E)$ between pairs of fluorescent spots as a function of their distance from each other Δd . a) Raw data compiled from 5 images acquired at 12 mm and b) at 22 mm along each of four different gradients. c) and d) Mean ΔE values as a function of separation between fluorescent spots. e) and f) Number of measurements along the gradients at the 12 and 22 mm positions. The large population near $\Delta d = 0$ is due to blinking of immobile single molecules. These results reveal a correlation in E values over distances of less than ~ 200 nm.

The width of the distribution obtained from blinking molecules (Figure 7e,f) near $\Delta d=0$ reflects the precision at which the individual molecules can be located. A fit of each distribution in this region (see blue lines in Figure 7e,f) yield widths consistent with ~ 40 - 70 nm single molecule localization precisions along the gradient. Therefore, blinking alone should cause an apparent correlation in E values that decays over distances of ~ 60 - 100 nm. In fact, the correlations in E values depicted in Figure 7c,d, and at the other positions along the gradient (see Supporting Information) all decay over two-to-three-fold larger distances. These results suggest that the acid/base properties of the gradients, as probed by the Nile Red molecules remain correlated over ~ 200 nm. The origins of such correlations are currently unknown, but may reflect the formation of domains with different densities of amine or silanol groups on the

gradient surface, or they may reflect the average distance over which surface bound amine groups can interact with silanol sites, altering their protonation states. They are not expected to derive from the finite localization precision of the single molecule measurements, because of the differences in the observed spatial extents of the artifacts due to blinking molecules in Figure 7e,f and the observed decay of the correlation in *E* shown in Figure 7c,d.

As a final point, it should be noted that the acid and base strengths expected for the materials investigated are consistent with the interpretations given above. While the pK_a values of protonated organic amines are typically $\sim 10.5,^{50}$ surface-bound ammonium groups have been found to be much more acidic, with pK_a $\sim 7.^{11}$ Likewise, the pK_a of surface silanol groups have been shown to fall in the range of ~ 4.5 - 8.5, with the majority of such sites having pK_a $\sim 8.5.^{51}$ Finally, while the pK_a of protonated Nile Red is difficult to determine because of its limited water solubility, it is likely somewhat more acidic than the pyridinium ion (pKa ~ 5.2).⁴⁷ The results reported in this work suggest that the amine groups should effectively compete for protons at the high-amine end, while at the low-amine end, it is the most acidic silanol sites that interact with the Nile Red molecules.

CONCLUSIONS

In summary, the application of Nile Red in single molecule spectroscopy studies of the local properties of bifunctional acid-base silica film gradients has been demonstrated for the first time. These studies rely upon the demonstrated response of Nile Red to the acidity of its local environment, rather than its usual solvent polarity dependence. The single molecule results were shown to be consistent with XPS mapping data obtained along similar gradients. The results show that the acidity/basicity properties of aminosilane gradients are dominated by the basic amine groups at the high-amine end of the gradient and by acidic silanol sites at the low-amine

end. Based on the XPS data, the fraction of protonated amine groups on the gradient surface was shown to increase running down the gradient as the density of acidic silanol sites increased. Likewise, based on the single molecule results, the fraction of protonated Nile Red molecules was also found to increase from the high- to low-amine ends of the gradient. Using the ability to locate the single molecules with ~ 50 nm precision, spatial correlations in the acidity/basicity properties of the aminosilane gradients were shown to occur over ~ 200 nm length scales. These correlations were concluded to reflect either the appearance of domains on the gradient surface or the distances scales over which amine groups and silanol groups interact with each other in determining surface properties. The methods and results of this study will be useful in gaining a better understanding the nature of bifunctional acid-base silica films used in catalytic chemical reactions such as ubiquitous aldol condensations.

NOTES

The authors declare no competing financial interest.

ACKNOWLEDGEMENTS

The authors acknowledge the support from the U. S. National Science Foundation (CHE-1664664). The U.S. Department of Energy (DE-SC0002362) is also acknowledged for providing the optical microscope employed. Takashi Ito is thanked for providing access to the spectroscopic ellipsometer.

SUPPORTING INFORMATION

Additional information on prediction of E values, additional XPS data, single molecule data, the full set of ΔE results, and representative fluorescence videos. This information is available free of charge via the internet at http://pubs.acs.org.

REFERENCES

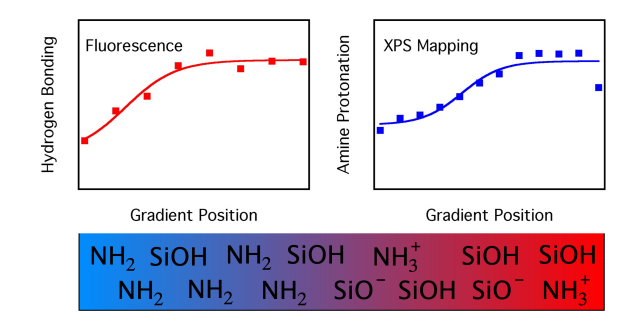
- (1) Margelefsky, E. L.; Zeidan, R. K.; Davis, M. E. Cooperative Catalysis by Silica-Supported Organic Functional Groups. *Chem. Soc. Rev.* **2008**, *37*, 1118-1126.
- (2) Zeidan, R. K.; Hwang, S. J.; Davis, M. E. Multifunctional Heterogeneous Catalysis: SBA-15-Containing Primary Amines and Sulfonic Acids. *Angew. Chem. Int. Ed.* **2006**, *45*, 6332-6335.
- (3) Collier, V. E.; Ellebracht, N. C.; Lindy, G. I.; Moschetta, E. G.; Jones, C. W. Kinetic and Mechanistic Examination of Acid-Base Bifunctional Aminosilica Catalysts in Aldol and Nitroaldol Condensations. *ACS Catal.* **2016**, *6*, 460-468.
- (4) Bass, J. D.; Solovyov, A.; Pascall, A. J.; Katz, A. Acid-Base Bifunctional and Dielectric Outer-Sphere Effects in Heterogeneous Catalysis: A Comparative Investigation of Model Primary Amine Catalysts. *J. Am. Chem. Soc.* **2006**, *128*, 3737-3747.
- (5) Morgenthaler, S.; Zink, C.; Spencer, N. D. Surface-Chemical and -Morphological Gradients. *Soft Matter* **2008**, *4*, 419-434.
- (6) Genzer, J. Surface-Bound Gradients for Studies of Soft Materials Behavior. *Annu. Rev. Mater. Res.* **2012**, *42*, 435-468.
- (7) Collinson, M. M.; Higgins, D. A. Organosilane Chemical Gradients: Progress, Properties, and Promise. *Langmuir* **2017**, *33*, 13719-13732.
- (8) Chaudhury, M. K.; Whitesides, G. M. How to Make Water Run Uphill. *Science* **1992**, *256*, 1539-1541.
- (9) Genzer, J.; Efimenko, K.; Fischer, D. A. Formation Mechanisms and Properties of Semifluorinated Molecular Gradients on Silica Surfaces. *Langmuir* **2006**, *22*, 8532-8541.
- (10) Ashraf, K. M.; Giri, D.; Wynne, K. J.; Higgins, D. A.; Collinson, M. M. Cooperative Effects in Aligned and Opposed Multicomponent Charge Gradients Containing Strongly Acidic, Weakly Acidic, and Basic Functional Groups. *Langmuir* **2016**, *32*, 3836-3847.
- (11) van der Vegte, E. W.; Hadziioannou, G. Acid-Base Properties and the Chemical Imaging of Surface-Bound Functional Groups Studied with Scanning Force Microscopy. *J. Phys. Chem. B* **1997**, *101*, 9563-9569.
- (12) Xu, W.; Kong, J. S.; Yeh, Y.-T. E.; Chen, P. Single-Molecule Nanocatalysis Reveals Heterogeneous Reaction Pathways and Catalytic Dynamics. *Nat. Mater.* **2008**, *7*, 992-996.
- (13) Zhang, Y.; Song, P.; Fu, Q.; Ruan, M.; Xu, W. Single-Molecule Chemical Reaction Reveals Molecular Reaction Kinetics and Dynamics. *Nat. Commun.* **2014**, *5*, 1-8.

- (14) Roeffaers, M. B. J.; Sels, B. F.; Uji-i, H.; De Schryver, F. C.; Jacobs, P. A.; De Vos, D. E.; Hofkens, J. Spatially Resolved Observation of Crystal-Face-Dependent Catalysis by Single Turnover Counting. *Nature* **2006**, *439*, 572-575.
- (15) Ristanović, Z.; Kubarev, A. V.; Hofkens, J.; Roeffaers, M. B. J.; Weckhuysen, B. M. Single Molecule Nanospectroscopy Visualizes Proton-Transfer Processes within a Zeolite Crystal. *J. Am. Chem. Soc.* **2016**, *138*, 13586-13596.
- (16) Brasselet, S.; Moerner, W. E. Fluorescence Behavior of Single-Molecule pH-Sensors. *Single Mol.* **2000**, *1*, 17-23.
- (17) Liu, X.; Chen, T.; Jain, P. K.; Xu, W. Revealing the Thermodynamic Properties of Elementary Chemical Reactions at the Single-Molecule Level. *J. Phys. Chem. B* **2019**, *123*, 6253-6259.
- (18) Fu, Y.; Collinson, M. M.; Higgins, D. A. Single-Molecule Spectroscopy Studies of Microenvironmental Acidity in Silicate Thin Films. *J. Am. Chem. Soc.* **2004**, *126*, 13838-13844.
- (19) Xie, J.; Xu, J.; Sun, X.; Wang, H.; Higgins, D. A.; Hohn, K. L. Exploring Microenvironment Acidity Inside the Solvent-Filled Pores of Mesoporous Silica Thin Films via Single-Molecule Spectroscopy. *J. Phys. Chem. C* **2019**, *123*, 20333-20341.
- (20) Sun, X.; Xie, J.; Xu, J.; Higgins, D. A.; Hohn, K. L. Single-Molecule Studies of Acidity Distributions in Mesoporous Aluminosilicate Thin Films. *Langmuir* **2015**, *31*, 5667-5675.
- (21) Deye, J. F.; Berger, T. A.; Anderson, A. G. Nile Red as a Solvatochromic Dye for Measuring Solvent Strength in Normal Liquids and Mixtures of Normal Liquids with Supercritical and Near Critical Fluids. *Anal. Chem.* **1990**, *62*, 615-622.
- (22) Lobnik, A.; Wolfbeis, O. S. Probing the Polarity of Sol-Gels and Ormosils via the Absorption of Nile Red. *J. Sol-Gel Sci. Tech.* **2001**, *20*, 303-311.
- (23) Lakowicz, J. R.: *Principles of Fluorescence Spectroscopy*; Second ed.; Kluwer Academic/Plenum Publishers: New York, 1999. pp. 185-194.
- (24) Hess, C. M.; Riley, E. A.; Palos-Chávez, J.; Reid, P. J. Measuring the Spatial Distribution of Dielectric Constants in Polymers through Quasi-Single Molecule Microscopy. *J. Phys. Chem. B* **2013**, *117*, 7106-7112.
- (25) Dickson, R. M.; Norris, D. J.; Tzeng, Y.-L.; Sakowicz, R.; Goldstein, L. S. B.; Moerner, W. E. Single Molecules Solvated in Pores of Polyacrylamide Gels. *Mol. Cryst. Liq. Cryst.* **1996**, *291*, 31-39.
- (26) Hou, Y.; Bardo, A. M.; Martinez, C.; Higgins, D. A. Characterization of Molecular Scale Environments in Polymer Films by Single Molecule Spectroscopy. *J. Phys. Chem. B* **2000**, *104*, 212-219.

- (27) Bardo, A. M.; Collinson, M. M.; Higgins, D. A. Nanoscale Properties and Matrix-Dopant Interactions in Dye-Doped Organically Modified Silicate Thin Films. *Chem. Mater.* **2001**, *13*, 2713-2721.
- (28) Giri, D.; Hanks, C. N.; Collinson, M. M.; Higgins, D. A. Single-Molecule Spectroscopic Imaging Studies of Polarity Gradients Prepared by Infusion-Withdrawal Dip-Coating. *J. Phys. Chem. C* **2014**, *118*, 6423-6432.
- (29) Kumarasinghe, R.; Ito, T.; Higgins, D. A. Nanoconfinement and Mass Transport in Silica Mesopores: the Role of Charge at the Single Molecule and Single Pore Levels. *Anal. Chem.* **2020**, *92*, 1416-1423.
- (30) Xu, H.; Nagasaka, S.; Kameta, N.; Masuda, M.; Ito, T.; Higgins, D. A. Spectroscopic Imaging Studies of Nanoscale Polarity and Mass Transport Phenomena in Self-Assembled Organic Nanotubes. *Phys. Chem. Chem. Phys.* **2017**, *19*, 20040-20048.
- (31) Sebok-Nagy, K.; Miskolczy, Z.; Biczók, L. Interaction of 2-Hydroxy-Substituted Nile Red Fluorescent Probe with Organic Nitrogen Compounds. *Photochem. Photobiol.* **2005**, *81*, 1212-1218.
- (32) Selivanov, N. I.; Samsonova, L. G.; Artyukhov, V. Y.; Kopylova, T. N. Theoretical and Experimental Investigations of Photophysics on the Nile Red Molecule and Its Protonated Structures. *Russ. Phys. J.* **2011**, *54*, 601-606.
- (33) Chen, T.; Dong, B.; Chen, K.; Zhao, F.; Cheng, X.; Ma, C.; Lee, S.; Zhang, P.; Kang, S. H.; Ha, J. W.; Xu, W.; Fang, N. Optical Super-Resolution Imaging of Surface Reactions. *Chem. Rev.* **2017**, *117*, 7510-7537.
- (34) Li, Z.; Ashraf, K. M.; Collinson, M. M.; Higgins, D. A. Single Molecule Catch and Release: Potential-Dependent Plasmid DNA Adsorption along Chemically Graded Electrode Surfaces. *Langmuir* **2017**, *33*, 8651-8662.
- (35) Stadler, A. F.; Melchior, T.; Müller, M.; Sage, D.; Blu, T.; Unser, M. Low-Bond Axisymmetric Drop Shape Analysis for Surface Tension and Contact Angle Measurements of Sessile Drops. *Colloids Surf. A.* **2010**, *364*, 72-81.
- (36) Tran Ba, K. H.; Everett, T. A.; Ito, T.; Higgins, D. A. Trajectory Angle Determination in One Dimensional Single Molecule Tracking Data by Orthogonal Regression Analysis. *Phys. Chem. Chem. Phys.* **2011**, *13*, 1827-1835.
- (37) Kumarasinghe, R.; Higgins, E. D.; Ito, T.; Higgins, D. A. Spectroscopic and Polarization-Dependent Single-Molecule Tracking Reveal the One-Dimensional Diffusion Pathways in Surfactant-Templated Mesoporous SIlica. *J. Phys. Chem. C* **2016**, *120*, 715-723.
- (38) Zhu, M.; Lerum, M. Z.; Chen, W. How to Prepare Reproducible, Homogeneous, and Hydrolytically Stable Aminosilane-Derived Layers on Silica. *Langmuir* **2012**, *28*, 416-423.

- (39) Zeng, X.; Xu, G.; Gao, Y.; An, Y. Surface Wettability of (3-Aminopropyl)triethoxysilane Self-Assembled Monolayers. *J. Phys. Chem. B* **2011**, *115*, 450-454.
- (40) Moses, P. R.; Wier, L. M.; Lennox, J. C.; Finklea, H. O.; Lenhard, J. R.; Murray, R. W. Xray Photoelectron Spectroscopy of Alkylamine-Silanes Bound to Metal Oxide Electrodes. *Anal. Chem.* **1978**, *50*, 576-585.
- (41) Sherwood, P. M. A. The Use and Misuse of Curve Fitting in the Analysis of Core X-ray Photoelectron Spectroscopic Data. *Surf. Interface Anal.* **2019**, *51*, 589-610.
- (42) Stuart, M. C. A.; van de Pas, J. C.; Engberts, J. B. F. N. The Use of Nile Red to Monitor the Aggregation Behavior in Ternary Surfactant-Water-Organic Solvent Systems. *J. Phys. Org. Chem.* **2005**, *18*, 929-934.
- (43) Carmichael, A. J.; Seddon, K. R. Polarity Study of Some 1-Alkyl-3-Methylimidazolium Ambient-Temperature Ionic Liquids with the Solvatochromic Dye, Nile Red. *J. Phys. Org. Chem.* **2000**, *13*, 591-595.
- (44) Datta, A.; Mandal, D.; Pal, S. K.; Bhattacharyya, K. Intramolecular Charge Transfer Processes in Confined Systems. Nile Red in Reverse Micelles. *J. Phys. Chem. B* **1997**, *101*, 10221-10225.
- (45) Sackett, D. L.; Wolff, J. Nile Red As a Polarity-Sensitive Fluorescent Probe of Hydrophobic Protein Surfaces. *Anal. Biochem.* **1987**, *167*, 228-234.
- (46) Li, Z.; Kumarasinghe, R.; Collinson, M. M.; Higgins, D. A. Probing the Local Dielectric Constant of Plasmid DNA in Solution and Adsorbed on Chemically Graded Aminosilane Surfaces. *J. Phys. Chem. B* **2018**, *122*, 2307-2313.
- (47) *Handbook of Chemistry and Physics*: 82nd ed.; Lide, D. R., Ed.; CRC Press: Boca Raton, 2001. p. 8-127.
- (48) Riddick, J. A. Acid-Base Titrations in Nonaqueous Solvents. *Anal. Chem.* **1956**, *28*, 679-687.
- (49) Kolling, O. W. Red Shift for Solvatochromic Indicators as a Measure of Solvent Basicity in Polar Aprotic Media. *Anal. Chem.* **1976**, *48*, 884-886.
- (50) Hall, H. K. Correlation of the Base Strengths of Amines. *J. Am. Chem. Soc.* **1957**, 79, 5441-5444.
- (51) Ong, S.; Zhao, X.; Eisenthal, K. B. Polarization of Water Molecules at a Charged Interface: Second Harmonic Studies of the Silica/Water Interface. *Chem. Phys. Lett.* **1992**, *191*, 327-335.

TOC ART



Supporting Information

Single Molecule Spectroscopy Studies of Acid-Base Chemical Gradients using Nile Red as a Probe of Local Surface Acidity

Abdulhafiz Usman^a, Shelby L. Weatherbee^b, Maryanne M. Collinson^b, Keith L. Hohn^{a,c,*}, Daniel A. Higgins^{d,*}

^aDepartment of Chemical Engineering, Kansas State University, Manhattan, KS 66506 ^bDepartment of Chemistry, Virginia Commonwealth University, Richmond, VA 23284 ^cDepartment of Chemical, Paper, and Biomedical Engineering, Miami University, Oxford, OH 45056

^dDepartment of Chemistry, Kansas State University, Manhattan, KS 66506

A description of how the E values for Nile Red in ethyl acetate and acetic acid solution were predicted is provided. Also included are XPS data from uniform (nongradient) aminosilane and silica films, along with single molecule spectroscopic data acquired from Nile Red dispersed on a uniform silica film. The full set of ΔE results (see Figure 7) obtained along the entire length of the aminosilane gradient samples are also provided. Representative single molecule videos are included.

^{*}Corresponding author emails: higgins@ksu.edu and hohnkl@miamioh.edu

Estimation of E values for Nile Red in ethyl acetate and acetic acid.

The E values expected for Nile Red in different solvent media are approximately related to the dielectric constant, ε , of the solvent, as defined in Eqn. S1:¹

$$E = K\left(\frac{\varepsilon - 1}{2\varepsilon + 1}\right) + C \tag{S1}$$

In this empirical relationship, K and C are constants that must be determined by experimental measurement of E using a series of solvent mixtures having different dielectric constants. Due to the approximate and phenomenological nature of this equation, the ε values employed in determining K and C have been estimated under the assumption of a simple linear relationship between the composition of a solvent mixture and its dielectric constant. Here, the data presented in a previous manuscript were used as a means to estimate K and C at 3.48 ± 0.13 and -0.92 ± 0.04 , respectively, from a series of ethanol/hexane mixtures. Using ε values for ethyl acetate and acetic acid of 6.08 and 6.20, in Eqn. S1, a difference in E of < 0.01 units is predicted for these two solvents. Note that the values of E predicted for ethyl acetate and acetic acid using the E and E values given above are far from the values observed in Figure 3 due to the different intermolecular interactions that occur in different solvents in general, and the participation of hydrogen bonding in the presence of acetic acid, in particular.

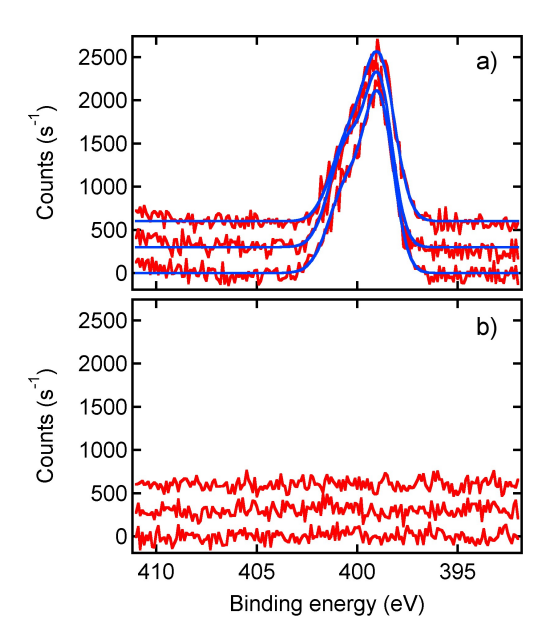


Figure S1. a) XPS spectra (red lines) of N1s peaks recorded on a uniform aminosilane film at \sim 8.5 mm spacings, beginning \sim 1.5 mm from the film edge. Each spectrum was fit to a pair of Gaussian functions (blue lines) centered at binding energies of 398.9 eV and 400.5 eV, which are assigned to the unprotonated and protonated forms of the aminosilane nitrogen, respectively. b) N1s spectra obtained from a silica baselayer in the absence of an aminosilane film at \sim 8.5 mm spacings, beginning \sim 1.5 mm from the film edge. The background-subtracted spectra in each series have been offset from zero to allow for better visualization.

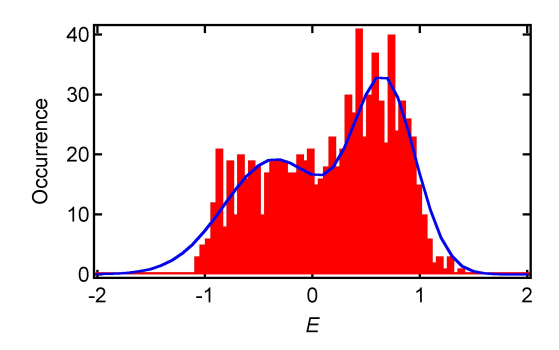


Figure S2. Histogram depicting the single molecule emission ratio (red bars) on a uniform silica film and its fit to a two component Gaussian distribution (blue line).

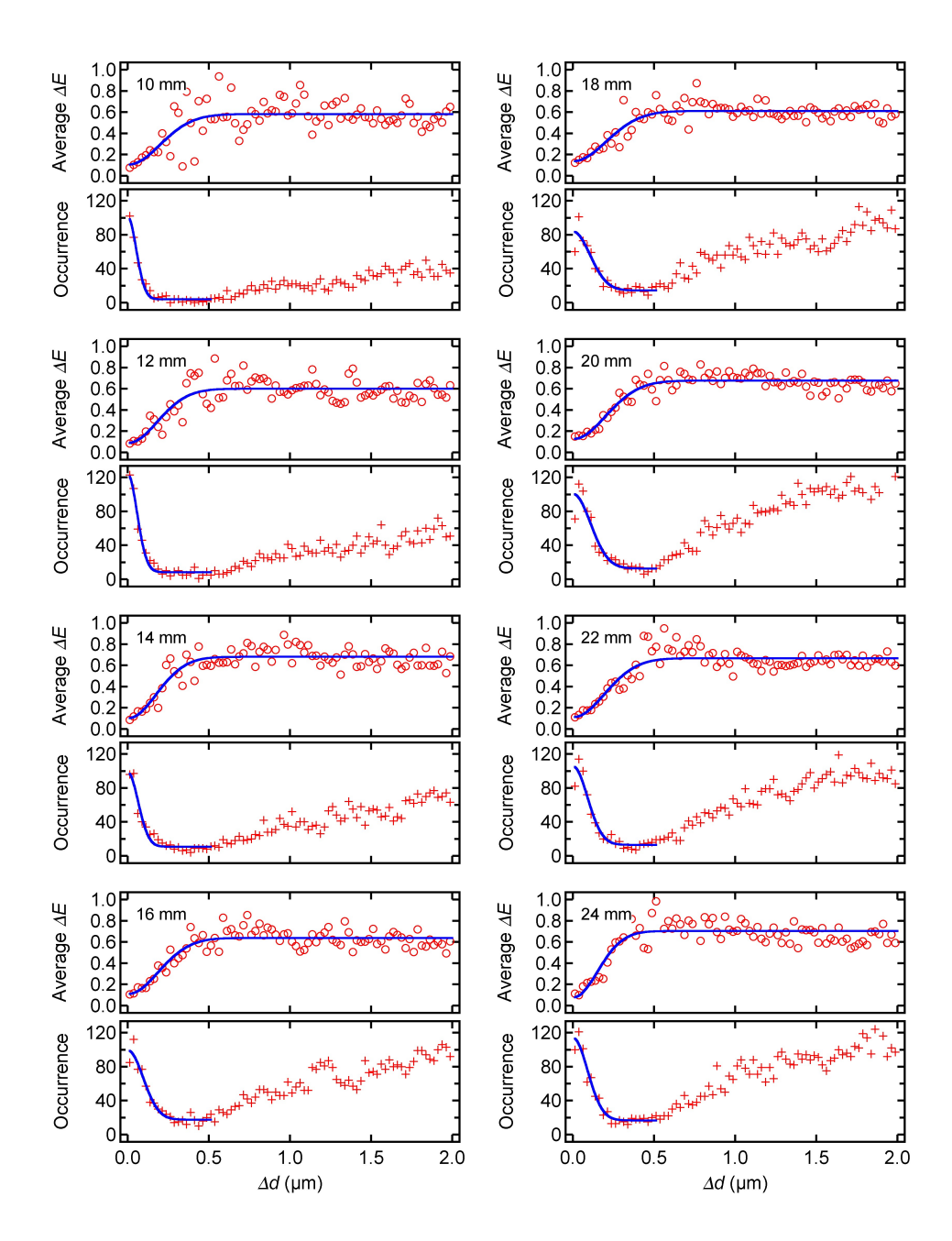


Figure S3. In pairs: difference in E (ΔE) between pairs of fluorescent spots and number of measurements as a function of their distance from each other, along the full gradient length. The large population near $\Delta d = 0$ is due to blinking of immobile single molecules. These results reveal a correlation in E values over distances of less than ~ 200 nm.

Video S1. Fluorescence video (50 frames, ~2 frames/s) depicting Nile Red dye molecules at the 10 mm position (high amine end) along the aminosilane gradient. The image data shown in Figure 5 were derived from this video. The left half displays the video acquired in the 580 nm channel while the right half display the video acquired in the 640 nm channel.

Video S2. Fluorescence video (50 frames, ~2 frames/s) depicting Nile Red dye molecules at the 24 mm position (low amine end) along the aminosilane gradient. The image data shown in Figure 5 were derived from this video. The left half displays the video acquired in the 580 nm channel while the right half display the video acquired in the 640 nm channel.

REFERENCES

- (1) Giri, D.; Hanks, C. N.; Collinson, M. M.; Higgins, D. A. Single-Molecule Spectroscopic Imaging Studies of Polarity Gradients Prepared by Infusion-Withdrawal Dip-Coating. *J. Phys. Chem. C* **2014**, *118*, 6423-6432.
- (2) *Handbook of Chemistry and Physics*: 82nd ed.; Lide, D. R., Ed.; CRC Press: Boca Raton, 2001. p. 8-127.